Applying Ferromagnetic Iron Spin Dynamics Methods to Uranium Dioxide

Anthony Lonsdale

Advisor: Dr. Aleksandr Chernatynskiy,

Physics Department

April 4th, 2022

Abstract Experiments conducted on Uranium Dioxide (UO_2) under the Manhattan Project led to the creation of the first self-sustaining nuclear reaction at Chicago-Pile 1 in 1942. Eighty years later, UO_2 functions as the primary fuel for nuclear fission reactors, providing around 10% of global electric output [1]. The importance of understanding UO_2's thermal and magnetic properties is instrumental in ensuring safe operation and handling, which can be done computationally using the Large-scale Atomic/Molecular Massively Parallel Simulator (LAMMPS). Simulating spin-lattice coupling with LAMMPS requires the usage of magneto-mechanical potentials instead of classical potentials, which captures more of the relevant quantum-mechanical physics that is dominant in low-temperature magnetic subsystems. UO_2 at low temperatures contains a non-trivial magnetic subsystem which is believed to be a result of quadrupole-quadrupole, magnetic exchange, and phonon-magnon interactions. We discuss progress made with simulating the magnetic subsystem of elemental Iron and possible applications to the technologically important material, UO_2.

Introduction UO_2 as it exists in nature is a black semiconducting powder, which has unusual thermal properties that have been the topic of studies conducted since the 1960s [2]. The typical nuclear fuel rod used in a fission reactor consists of a stack of small sintered UO_2 pellets with Zirconium metal cladding to resist heat and chemical damage. The thermal conductivity of the dense UO_2 solid decreases as the metal's temperature rises, contrasting with the conductivity of the Zirconium cladding which increases as its temperature rises. Achieving a proper balance with these two materials is difficult, and for many reactor applications, particularly designs that NASA produces, Uranium Nitride (UN) is utilized for its superior thermal conductivity properties and higher melting point. Consistent efforts are being invested into increasing the thermal conduction of nuclear fuel via the usage of dopants due to their effect on the efficiency of heating up reactor baths [3].

The thermal conductivity of the cubic fluorite structure of molecular UO_2 is described using Fourier's Law, $J_z = -k_z \frac{dT}{dz}$, where J_z represents heat flux, k_z represents the thermal conduction coefficient, and $\frac{dT}{dz}$ represents thermal gradient, and z represents the crystallographic direction. A past study conducted by A. Lonsdale verified the isotropic nature of UO_2 in the 300 Kelvin regime using LAMMPS classical potentials [4]. Below 300 Kelvin, quantum-mechanical effects begin to significantly impact the thermal properties of UO_2, especially as the magnetic phase shift from paramagnetism to antiferromagnetism occurs below the Neél point of 30.8 Kelvin. To include the effect of magnetism on the thermal properties of UO_2, magneto-mechanical potentials must be used in MD simulations over the temperature range of 50-1000 Kelvin. Magneto-mechanical potentials are currently unavailable for UO_2; therefore, we investigate this effect in elemental iron. This study elucidates the magnitude and effects of magnetic spin substructures on the thermal conductivity of elemental iron, with the possible application to the UO_2 regime.

Methods Spin Dynamics (SD) simulations which involved the usage of the direct method were used to calculate lattice thermal conductivity for Iron [5]. The SPIN package, developed in 2018 by Tranchida et al. [6], utilizes a coupled spin-lattice approach to generate a molecular lattice structure of the Iron system with greater accuracy than using standard short-range MD code. Mishin's 2006 Interatomic potentials including exchange interaction used for the Iron system and were sourced from the LAMMPS Interatomic Potential Database [7], [8], [9]. These potentials accurately reproduce the lattice properties for both the BCC and high-temperature FCC phases of the metal and capture the relevant phonon interactions present at low temperatures.

A constant heat flow of 1 eV/ps was imposed in a rectangular cuboid simulation cell by conducting thermal energy from hot and cold plates separated by one-half of the simulation cell length. The thickness of one bcc Fe unit cell measures 2.867 Å. Periodic boundary conditions were applied to the simulation cell. The size of the time step was 1.0 fs in all simulations. Equilibration of thermal and strain properties of the systems was achieved by performing constant temperature (NVE) and constant pressure (NPT) simulations for 300ps. The data acquisition period for the heat flow was 600-10,000 ps. The heat flux of the system was averaged over the data acquisition period and was used to calculate the lattice thermal conductivity via Fourier's Law.

The length of the simulation cells ranged from 40 to 320nm along the <100> crystallographic direction. Results for infinite cell length was obtained by the extrapolation of $\frac{1}{\kappa} = \frac{1}{\kappa_\infty} + \frac{1}{L_z}$, where L_z is the length of the simulation and κ_∞ is the thermal conductivity for a simulation cell of infinite length. In the direction parallel to the thermal current, the height and width of the simulation cell is 28.67 Å. Four different systems were measured, exchange-disabled, positive exchange interaction (ferromagnetic), positive exchange interaction at one-third strength, and negative exchange interaction (antiferromagnetic). Systems with lattice temperatures ranging from 50-1000 Kelvin were measured. The inter-atomic forces between iron atoms were described by short-range exchange interaction forces calculated using the embedded atom method. Possible anisotropy of the thermal conductivity tensor for all iron systems was not considered.

Pairwise interactions, otherwise referred to as magneto-mechanical potentials, for the Iron metal were computed using the embedded-atom method (EAM) with the total energy of an arbitrary atom given by the following expression:

$$E_i = F_\alpha \left(\sum_{j \neq i} \rho_\beta (r_{ij}) \right) + \frac{1}{2} \sum_{j \neq i} \phi_{\alpha\beta} (r_{ij}) \tag{1}$$

where F_α is the embedding energy, which is a function of the atomic electron density, rho, phi is the pair interaction energy and alpha and beta are the element types of atoms I and J [10]. Both summations in the formula are computed over all neighbors J of atom I within a specified cutoff

distance, which is 1.841 Å in this study. For the Iron system, the formula reduces to simply the atomic electron density summation. Application to the UO_2 system requires the specification of three functions, $\phi(r), \rho(r)$ and $F(\rho)$, which are dependent on understanding the complex quadrupole-quadrupole, spin-exchange, and phonon-magnon (lattice vibration) interactions, which cannot currently be handled automatically by LAMMPS.

Generation of the iron lattice structure using the LAMMPS SPIN package was performed by computation of the coupled spin-lattice Hamiltonian as shown:

$$\boldsymbol{H}_{sl} = \underbrace{\sum_{i=1}^{N} \frac{|\boldsymbol{p}_i|^2}{2m_i} + \sum_{i,j=1}^{N} V(r_{ij})}_{MD\ Hamiltonian} \underbrace{- \sum_{i,j,i \neq j}^{N} J(r_{ij})\, \vec{s}_i * \vec{s}_j - \mu_B \mu_0 \sum_{i=0}^{N} g_i \vec{s}_i * \boldsymbol{H}_{ext}}_{Spin-lattice\ coupling} \qquad (2)$$

where terms one and two in the RHS of Eq. 1 represent the classical potential energies resulting from atomic momentum and coulombic long and short-ranged interactions, respectively. Term three in Eq. 2 represents the spin-exchange interaction, responsible for the local alignment of neighboring atomic spins which produces ferromagnetism and antiferromagnetism, among other magnetic phases. Term four, the Zeeman term, represents any influences from external magnetic fields on atomic magnetic spins, of which a field strength of 1 Tesla was used for this study to align spins at timestep 0.

The spin-exchange interaction term present in Eq. 2 is by far the most dominant quantum-mechanical effect present in low-temperature iron lattices and is also relevant in the low-temperature UO_2 system. The exchange interaction is defined between pairs of magnetic spins as the following summation of pairs of nearest neighbors:

$$\boldsymbol{H}_{exchange} = - \sum_{i,j,i \neq j}^{N} J(r_{ij})\, \vec{s}_i * \vec{s}_j \qquad (3)$$

where the neighboring magnetic spin moments of atoms i and j are represented as unit vectors and $\vec{s}_j$, and $r_{ij} = |\vec{r}_i - \vec{r}_j|$ is the interatomic distance between these two atoms. The Heisenberg exchange coupling function, $J(r_{ij})$, defines the magnitude and the sign of the spin-exchange interaction for different neighboring shells, with a negative term simulating antiferromagnetism and a positive term simulating ferromagnetism. It is important to note that $J(r_{ij})$ is dependent on interatomic distance, and is generally a radial function, so no anisotropic effect can be modelled using this method. From the exchange interaction defined in Eq. 3, each spin i will be submitted to a magnetic torque $\vec{\omega}_i$ and its associated atom can be submitted to a force $\vec{F}_i$ for spin-lattice calculations such as the following:

$$\vec{\omega}_i = \frac{1}{\hbar} \sum_{j}^{Neighbor} J(r_{ij})\, \vec{s}_j \ and \ \vec{F}_i = \sum_{j}^{Neighbor} \frac{\partial J(r_{ij})}{\partial r_{ij}} (\vec{s}_i * \vec{s}_j)\, \vec{e}_{ij} \qquad (4)$$

where $\hbar$ is Planck's constant and $\vec{e}_{ij} = \frac{\vec{r}_i - \vec{r}_j}{|\vec{r}_i - \vec{r}_j|}$ is the unit vector between neighboring sites i and j.

LAMMPS simulations using the exchange interaction consist of an iterative three-step integration algorithm when calculating the motion of each individual atom in the molecular lattice structure. Operation one applies a precession torque to each magnetic spin in the group, which is determined by the Zeeman term in the RHS of Eq. 2. Operation two accounts for temperature effects from operation one by connecting every atomic spin to a thermal bath with the usage of a Langevin thermostat. This operation performs Brownian dynamics (BD) where a random torque and a transverse dissipation are applied to each spin according to the stochastic Landau-Lifshitz-Gilbert equation. Operation three performs a symplectic integration with a micro-canonical ensemble (NVE) for the spin-lattice system which accounts for motion effects. A "moving" lattice was used for the integration of the spins over both spin and atomic degrees of freedom to capture the spin-lattice coupling of iron.

Magnetization data was retrieved from all simulations and followed expected magnetic phase behavior, displaying proper ferromagnetic, antiferromagnetic, and paramagnetic spin structures as the systems approached the Curie point of iron. Phase transitions occurred at their respective temperatures as determined by the spin-exchange interactions.

Results The magnetic phases as shown in Fig. 1 reflect accurately the expected magnetic phases for a molecular iron lattice, with the underlying magnetic subsystem behaving appropriately. The magnetic subsystem results give us higher confidence in the accuracy of the thermal transport measurements for the iron systems.
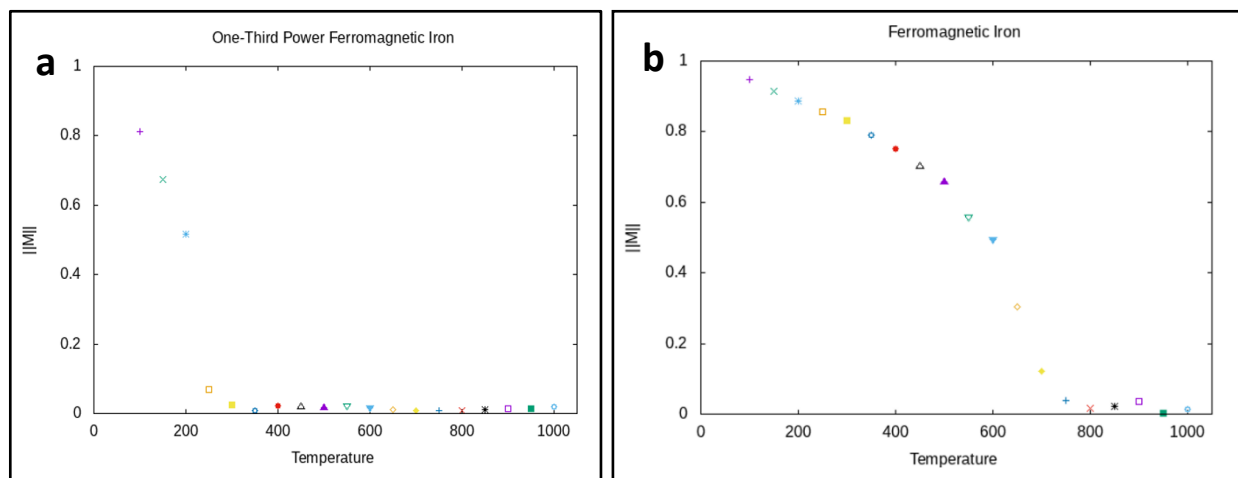

Figure 1 | Normalized Magnetic Moments for Ferromagnetic Systems. The magnitude of the magnetic moments from the two important ferromagnetic systems is shown, with the magnetic moment of the antiferromagnetic system near zero for all temperatures. **(a)** Inset shows the Curie point reached around 200 Kelvin for the one-third strength exchange interaction with ferromagnetic behavior transitioning to paramagnetic behavior for the iron system. **(b)** Inset shows the Curie point of around 800 Kelvin for the regular iron system with a full-strength exchange interaction.
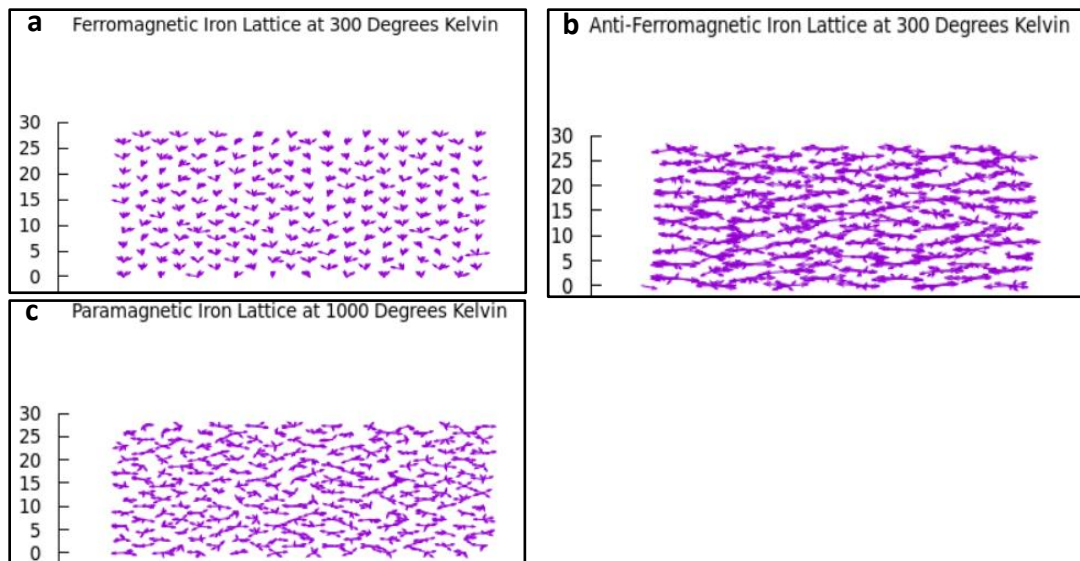
Figure 2 | Structure of Magnetic Subsystems. Magnetic spin vectors on each atom are shown in a side profile view of the iron molecular lattice. **(a)** Inset shows a parallel orientation of atomic magnetic spins consistent with ferromagnetic phase. **(b)** Inset shows the anti-parallel orientation of atomic magnetic spins consistent with antiferromagnetic phase. **(c)** Inset shows random orientations of atomic magnetic spins at a high temperature consistent with paramagnetic phase.

Several non-trivial and unique effects are on display as we look at the overall data for the Lattice Thermal Conductivity. The magnitude of the thermal conductivity is largest for the full-strength ferromagnetic system, with the one-third strength system being slightly lower. The anti-ferromagnetic system appears to have a reduced thermal conductivity, the reason for which may be because of heat energy being dissipated due to the anti-alignment of magnetic spins, which impedes phonon and magnon transport through the molecular lattice. The magnitude of the thermal conductivity change approaches a minimum as the lattices reach their respective Curie points and the magnetic substructure becomes disordered.
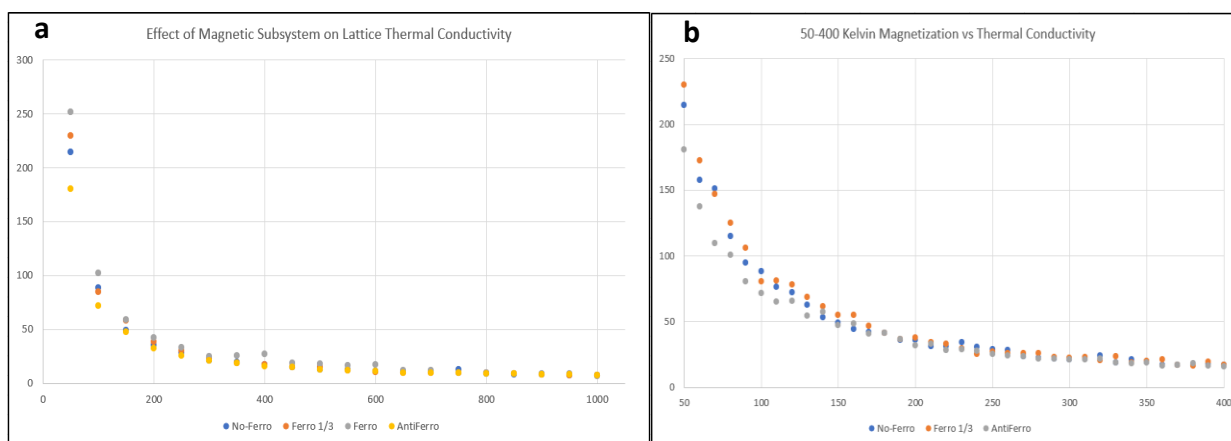

Figure 3 | Effect of Magnetic Subsystem on Lattice Thermal Conductivity. Magnetized systems are plotted with respect to thermal conductivity at discrete temperatures, extrapolated to

infinite system length. **(a)** Inset shows convergence as each system reaches their respective Curie point. **(b)** Inset shows enhanced resolution and significant dependence of magnetization at temperatures below 400 Kelvin. The magnitude of thermal conductivity is minimally affected for the one-third strength ferromagnetic system, approximately 13% larger for the ferromagnetic system on average, and approximately 0.7% smaller for the antiferromagnetic system on average.

Discussion The Spin-Lattice coupling approach captures more of the relevant physics surrounding thermal interactions in low-temperature molecular systems. The energy transferred from ballistic conduction, and the momentum carried by atomic magnetic spins in the system can theoretically be separated and the thermal conductivity of each component may be elucidated and calculated, however, this was not done for our study. Our results show a clear interaction between the magnetic subsystems and the thermal transport properties of Iron. The average error associated with the system size extrapolation for each temperature was reported as 1.62% for the spin-disabled system, 1.72% for the full-strength positive exchange interaction (ferromagnetic) system, 1.09% for the one-third strength positive exchange interaction (ferromagnetic) system, and 1.56% for the negative exchange interaction (antiferromagnetic) system.

Ab Initio methods must be applied to the UO_2 system to determine the effect of magnetism on thermal conductivity, as a proper definition of the magneto-mechanical potentials and low-temperature magnetic subsystem behavior does not exist. Reproduction of the simulation of the iron systems for the UO_2 system using the methodology laid out in this study can lead to a determination of the experimental question.

References

1. Wang, Lian & Kaye, M. (2020). Oxide power reactor fuels. 10.1016/B978-0-08-102571-0.00005-7.
2. Thermal conductivity of uranium dioxide, Report of the Panel on Thermal Conductivity of Uranium Dioxide held in Vienna, 26-30 April 1965. 68 p. (IAEA, Technical reports series no. 59)
3. Jennifer K. Watkins, et al. Enhancing thermal conductivity of UO2 with the addition of UB2 via conventional sintering techniques, J. Nucl. Mater., 559, (2022), ISSN 0022-3115
4. Lonsdale, Anthony & Chernatynskiy, Aleksandr, "Effect of Magnetic Moment on Thermal Conductivity" (2021). Undergraduate Research Conference at Missouri S&T. 8.
5. Schelling, P. K., Phillpot, S. R. & Keblinski, P. Comparison of atomic-level simulation methods for computing thermal conductivity. Phys. Rev. B 65, 144306 (2002)
6. Tranchida, Plimpton, Thibaudeau and Thompson, massively parallel symplectic algorithm for coupled magnetic spin dynamics and molecular dynamics, J. Comp. Phys., 372, 406-425, (201o-m8).
7. C.A. Becker, F. Tavazza, Z.T. Trautt, and R.A. Buarque de Macedoc (2013), "Considerations for choosing and using force fields and interatomic potentials in materials science and engineering," Current Opinion in Solid State and Materials Science, 17, 277-283. DOI: 10.1016/j.cossms.2013.10.001
8. L.M. Hale, Z.T. Trautt, and C.A. Becker (2018), "Evaluating variability with atomistic simulations: the effect of potential and calculation methodology on the modeling of lattice and elastic constants," Modelling and Simulation in Materials Science and Engineering, 26, 055003. DOI: 10.1088/1361-651X/aabc05
9. H. Chamati, N.I. Papanicolaou, Y. Mishin, and D.A. Papaconstantopoulos (2006), "Embedded-atom potential for Fe and its application to self-diffusion on Fe(100)", Surface Science, 600(9), 1793-1803. DOI: 10.1016/j.susc.2006.02.010.
10. Daw, Baskes, Phys Rev Lett, 50, 1285 (1983). Daw, Baskes, Phys Rev B, 29, 6443 (1984).